Particle collisions control stable bed configuration under weak bedload transport conditions

Thomas C. Ashley[1], Suleyman Naqshband[2], Brandon McElroy[1]

[1]Department of Geology and Geophysics, University of Wyoming, Laramie, WY
[2]Department of Environmental Sciences, Wageningen University, Wageningen, Netherlands

Key Points:

- Experiments highlight differences in particle behavior over stable and unstable planar topography.
- Planar topography is unstable when particle collision events are more frequent than entrainment events.
- A theoretical stability field for lower-stage plane bed topography is proposed.

Corresponding author: Thomas C. Ashley, `tashley22@gmail.com`

Abstract

Sedimentary bed configurations that are stable under weak fluid-driven transport conditions can be divided into two groups: (1) meso-scale features that influence flow and sediment transport through roughness and drag partitioning effects ("mesoforms"), and (2) grain-scale features that can effectively be ignored at the macroscopic scale ("microforms"). These groups produce distinct sedimentary structures and are thought to be separated by transition in process regime characterized by the onset of nonlinear coarsening associated with flow separation and scour. However, the physical mechanisms responsible for this transition are poorly understood. Previous studies suggest that interactions between moving particles lead to stabilized bed disturbances that initiate nonlinear morphodynamic feedbacks. This study presents a quantitative interpretation of this hypothesis that is tested using experimental observations of particle motion over stable and unstable quasi-planar topography. We find that the microform/mesoform transition corresponds to the transition from rarefied to congested transport quantified by the dimensionless ratio of particle collision frequency to particle entrainment frequency. Combined with empirical relations for bedload flux and particle travel time, theory presented herein enables prediction of bed configuration under weak bedload transport conditions.

1 Introduction

Self-organized bedforms like ripples and dunes are essential equilibrium features of fluid driven sediment transport. Bedform dynamics are germane to problems in geomorphology, river engineering, and geology because they influence macroscopic flow and sediment transport through roughness and drag partitioning effects (Einstein, 1950; Engelund & Hansen, 1967; Smith & Mclean, 1977; Fredsoe, 1982; van Rijn, 1984; Wright & Parker, 2004; Best, 2005) and produce cross-bedded sedimentary architecture that can be used to interpret past flow conditions (Paola & Borgman, 1991; Leclair & Bridge, 2001; Mahon & McElroy, 2018; Leary & Ganti, 2020). They form under a wide range of conditions; however, planar or quasi-planar topography is thought to be stable under weak bedload transport conditions near the threshold of motion in sand and gravel (Leeder, 1980; Southard & Boguchwal, 1990; Van den Berg & Van Gelder, 1993; Best, 1996; Carling, 1999).

Predicting the occurrence of planar topography under weak bedload transport conditions is important from a practical standpoint because (a) grain roughness is the primary source of flow resistance (Engelund & Fredsoe, 1982), (b) sediment transport is efficient because energy is not lost to form drag (Wiberg & Smith, 1989), and (c) primary current stratification lacks recognizable cross-bedded structures (Leeder, 1980; Baas et al., 2016). Weak bedload transport conditions are common in rivers and are responsible for a significant fraction of fluvial stratigraphy due to quasi-universal relations governing the geometry of self-formed channels (Lacey, 1930; Schumm, 1960; S. Ikeda et al., 1988; Dade & Friend, 1998; Eaton et al., 2004; Parker et al., 2007; Wilkerson & Parker, 2010; Métivier et al., 2017; Dunne & Jerolmack, 2018). In practice, weak bedload transport conditions prevail in gravel bed rivers during floods and in sand bed rivers during low flows.

Despite being a geomorphically and geologically significant phenomenon, the mechanisms that determine whether planar topography is stable under specific flow conditions are poorly understood. Numerous studies describe turbulent flow and sediment transport processes during the initial phase of bedform initiation (Venditti et al., 2005a; Coleman & Nikora, 2009, 2011, references therein); however, these typically focus on flow conditions above the threshold of bedform development and neglect the mechanics of transport over stable plane beds. Theoretical stability analyses predict the occurrence of planar topography when mechanisms that attenuate topographic perturbations outpace amplification at every wavelength (Engelund & Fredsoe, 1982; McLean, 1990; Charru et al., 2013), but depend on continuum models that are incompatible with the rarefied nature of sediment transport near the threshold of motion (Furbish et al., 2017). As a result, they cannot capture grain-scale effects that many authors argue are an essential component of the bedform initiation process (Bagnold, 1935; Langbein & Leopold, 1968; Costello, 1974; Coleman & Melville, 1996; Coleman & Nikora, 2009). Attempts to delineate plane-bed stability fields empirically are hindered by overlapping observations of ripples, dunes and a suite of small-scale features like bedload sheets (Whiting et al., 1988; Best, 1996; Carling, 1999; Venditti et al., 2008), particle clusters (Best, 1996; Strom et al., 2004), and low-relief bedforms (H. Ikeda, 1983; Hubbell et al., 1987; Gomez et al., 1989; Best, 1996; Carling et al., 2005) that are thought to be distinct from well-developed ripples and dunes due to the absence of strong flow separation and scour at the point of reattachment (Best, 1996; Seminara et al., 1996; Carling, 1999; Carling et al., 2005).

The goal of this study is to clarify the mechanisms that control the onset of ripple and dune development from lower-stage plane bed (LSPB) topography under weak bedload transport conditions (Figure 1). As a starting point, we propose a definition of LSPB that encompasses quasi-planar "microforms" like bedload sheets, particle clusters, and other low-amplitude bedforms. In other words, we explicitly define LSPB as a macroscopic description of bed configuration characterized by the absence of well-developed ripples and dunes. We argue that this definition is appropriate because it is aligned with the practical considerations outlined above (related to flow, sediment transport, and stratigraphic architecture) and reflects a fundamental transition in process regime marked by the onset of nonlinear morphodynamic coarsening.

To elaborate this point, consider that a precise definition of LSPB must recognize that the the concept of planar topography breaks down at the granular scale. The random motion of particles driven by turbulent fluid flow causes disturbances in bed elevation (Leeder, 1980; Gyr & Schmid, 1989; Best, 1992) such that the minimum relief of a mobile bed undergoing active sediment transport is several times the nominal particle diameter (Whiting & Dietrich, 1990; Clifford et al., 1992). Rather than being completely uncorrelated, these disturbances tend organize into recognizable structures due to interactions between moving particles (i.e. "kinematic clumping", Bagnold, 1935; Langbein & Leopold, 1968; Costello, 1974; Venditti et al., 2006). In other words, particles aggregate into mobile clusters through viscous-damped collisions and produce localized disturbances in bed elevation when they come to rest (Coleman & Melville, 1994, 1996; Coleman & Eling, 2000; Coleman & Nikora, 2009, 2011). Microforms are likely an inevitable outcome of this process (Shinbrot, 1997).

Organized grain-scale bed disturbances may remain stable, or they may initiate pattern coarsening through nonlinear morphodynamic feedbacks. Previous studies observed the onset of significant flow separation behind disturbances (Williams & Kemp, 1971; Leeder, 1980; Best, 1996; Gyr & Kinzelbach, 2004) and defect propagation through scour-deposition waves (Raudkivi, 1963, 1966; Southard & Dingler, 1971; Costello & Southard, 1981; Gyr & Schmid, 1989; Best, 1992; Venditti et al., 2005a) when bed disturbances exceed a critical height of 2-4 particle diameters (Williams & Kemp, 1971; Leeder, 1980; Costello & Southard, 1981; Coleman & Nikora, 2009, 2011). We suggest that this threshold defines a transition in process regime that suitably differentiates morphodynamically-scaled "mesoforms" (ripples and dunes, *contra* Carling, 1999) from microforms that scale primarily with particle diameter. Below this threshold, the bed configuration may be assumed to be quasi-planar in practical applications because (a) mobile bed roughness models already include the effect of microforms (Whiting & Dietrich, 1990; Clifford et al., 1992), (b) flow separation is poorly developed such that drag partitioning effects can be ignored for the purposes of predicting sediment load, and (c) preserved cross-bedding structures have a maximum thickness of several particle diameters and are likely be indistinguishable from planar laminations in the rock record.

We hypothesize that interactions between mobile particles ("collisions") play a critical role in determining whether microforms achieve sufficient relief to initiate morphodynamic coarsening. Similar ideas have been promoted by numerous authors throughout the history of bedform research (Bagnold, 1935; Langbein & Leopold, 1968; Costello, 1974). Most recently, a series of papers by S. E. Coleman and others (Coleman & Melville, 1994, 1996; Coleman & Eling, 2000; Coleman & Nikora, 2009, 2011) argued that bedform initiation occurs when interactions between clusters of mobile particles cause a bed disturbance that interrupts the bedload layer. We present a precise kinematic interpretation of this hypothesis that is tested directly using experimental observations of tracer particle motion.

Topographic evolution occurs through the entrainment and disentrainment of individual sediment particles, thus, the morphodynamic importance of particle collisions may be evaluated by comparing the particle collision frequency Z_g ($\mathrm{L}^{-2}\mathrm{T}^{-1}$) (particle collision events per second per unit bed area) with the particle entrainment frequency E_g ($\mathrm{L}^{-2}\mathrm{T}^{-1}$) (particle entrainment events per second per unit bed area). The ratio $\theta = Z_g/E_g$ (henceforth, the "collision number"), characterizes the potential for particle collisions to influence topographic change and may be interpreted as the average number of particle collisions per particle transport event from entrainment to disentrainment. Thus, we hypothesize that LSPB is stable if $\theta < 1$, meaning collisions are rare and most transport events, or "hops", involve no collisions. As a corollary, we hypothesize that bedform initiation occurs when $\theta > 1$ such the collisions are frequent relative to exchanges with the bed.

In order to test this hypothesis, we compare particle entrainment and collision frequencies over stable and unstable planar topography. This is accomplished using digitized motions of tracer particles that comprise a known fraction of the bed material. Collision frequencies are estimated using using kinetic theory of gasses (Kauzmann, 2012), which has previously been used by Sommerfeld (2001) and Oesterle and Petitjean (1993) to describe particle collisions in turbulent flow, and by Bialik (2011) to predict collisions among saltating particles. We find that the transition from stable to unstable planar topography corresponds to the transition from rarefied to congested transport. This finding leads to an explicit theoretical prediction of the LSPB stability field in terms of particle Reynolds number and Shields stress that is consistent with observations compiled by Carling (1999).

2 Theory

Here, we present a simplified kinetic description of particle collisions assuming (a) the motion of each particle is independent of other particles, (b) that the bedload layer near the threshold of motion is thin such that particles may not move above or below one another without interacting (reducing the problem to two spatial dimensions), and (c) particle interactions occur when their surfaces come in contact and not before. Under these assumptions, the collision frequency depends on the concentration of particles in the bedload layer particles as well as their sizes and relative velocities (Sommerfeld, 2001). We recognize that these assumptions are not strictly valid because particle motions driven by turbulent fluid flow are not independent (Oesterle & Petitjean, 1993; Sommerfeld, 2001), the bedload layer may be several particle diameters thick (Wiberg & Smith, 1985; Wiberg, 1987), and particles influence each other without coming into into direct contact through viscous boundary layer and turbulent wake effects (Schmeeckle et al., 2001; Marshall, 2011). However, a simplified theoretical approach provides a first-order estimate of the relative importance of particle collisions. In principle, we assume that appropriate corrections are similar in both experiments and small relative to the primary effects considered here.

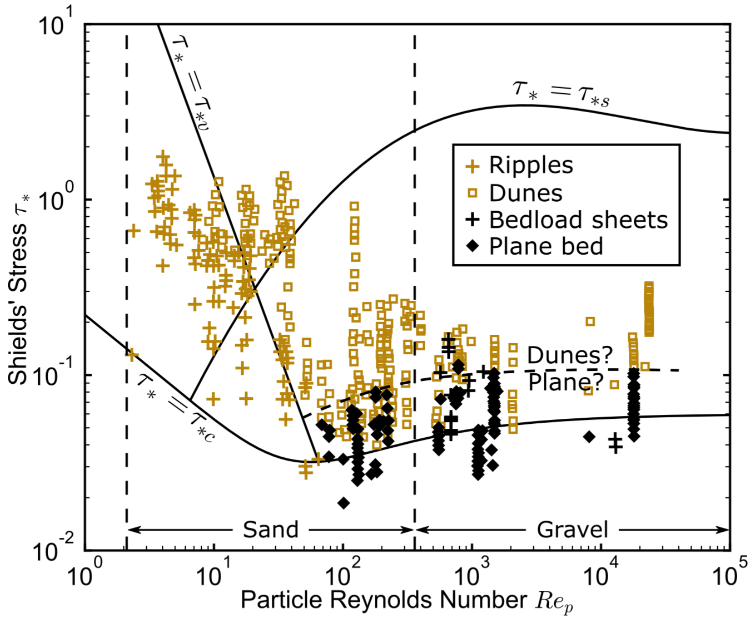

Figure 1. Shields-Parker river sedimentation diagram with empirical LSPB-Dune threshold (blue dashed line) adapted from García (2008). The observations of bed configuration reported by Carling (1999) are plotted for comparison. Here, τ_{*v} is the viscous threshold Shields stress (García (2008), Equation 2-78), τ_{*s} is the suspension threshold Shields stress (Equation 2-75), and τ_{*c} is the critical Shields stress for sediment motion (Equation 2-59a). Observations of ripples and dunes below the plane/dune transition may be low-amplitude features that are distinct from well-developed ripples and dunes following Best (1996), Seminara et al. (1996), and Carling et al. (2005).

Consider two circular particles with radius r moving in a 2-dimensional plane. The particles collide if their boundaries overlap; this occurs if their centers pass within a distance of $2r = D$. Thus, a single moving particle sweeps out a rectangle with width $2D$, called the "collision cross-section". The mean free path λ describes the average distance a particle may move before colliding with another particle and is given by:

$$\lambda = \frac{1}{2D\gamma_g} \tag{1}$$

where γ_g ($\mathrm{L}^{-2}\mathrm{T}^{-1}$) is average number of moving particles per unit bed area, referred to here as the granular particle activity. The reciprocal of the mean free path $2D\gamma_g$ may be interpreted as the average number of particles contained within a unit length rectangle of width $2D$.

If particle motions are independent, the long-term average collision frequency for a single particle may be estimated from the mean deviatoric speed, denoted by the shorthand $\tilde{u}_p = \langle ||\mathbf{u}_p - \langle \mathbf{u}_p \rangle|| \rangle$, where $\mathbf{u}_p$ is the instantaneous velocity vector, vertical lines denote vector magnitude and angle brackets denote averaging over the statistical-mechanical ensemble (Furbish et al., 2012). The mean deviatoric speed is the average speed a particle is moving relative to mean advective field. Kinetic theory predicts that an individual particle will experience an average of $\tilde{u}_p/\lambda$ collisions per unit time.

Finally, the collision frequency of all particles may be estimated from the collision frequency of a single particle. If there are γ_g moving particles per unit bed area, each of which experiences $\tilde{u}_p/\lambda$ collisions per unit time, then the average number of collisions per unit bed area per unit time is given by:

$$Z_g = \gamma_g \frac{\tilde{u}_p}{\lambda}. \tag{2}$$

Thus, θ may be estimated from parametric descriptions of particle motion as:

$$\theta = \frac{2D\tilde{u}_p\gamma_g^2}{E_g} \tag{3}$$

An alternative formulation can be obtained under steady, uniform macroscopic boundary conditions through the following equivalence:

$$E_g = \frac{\gamma_g}{T_p}, \tag{4}$$

where T_p is the average particle travel time. This expression can be obtained from the equivalent volumetric statement (Furbish et al., 2012, Equation E5) by dividing both sides by the nominal particle volume V_p (L^3). From (4), θ can be rewritten as

$$\theta = 2D\tilde{u}_p T_p \gamma_g = \frac{\tilde{u}_p T_p}{\lambda}. \tag{5}$$

A schematic interpretation of this expression is presented in Figure 2. Here, we note that $1/\theta$ is like a Knudsen number with characteristic length $\tilde{u}_p T_p$ (Furbish, 1997; Furbish et al., 2017; Rapp, 2017). The Knudsen number quantifies the transition from rarefied to congested transport, providing an alternative interpretation of our hypothesis; that is, plane-bed topography is stable when sediment transport is rarefied at the scale of individual particle hops and becomes unstable when the bedload layer behaves like a continuum.

3 Description of Experiments

3.1 Overview

Two laboratory flume experiments were conducted in order to test the hypothesis presented above. Our primary objective was to measure θ using Equation (3) under

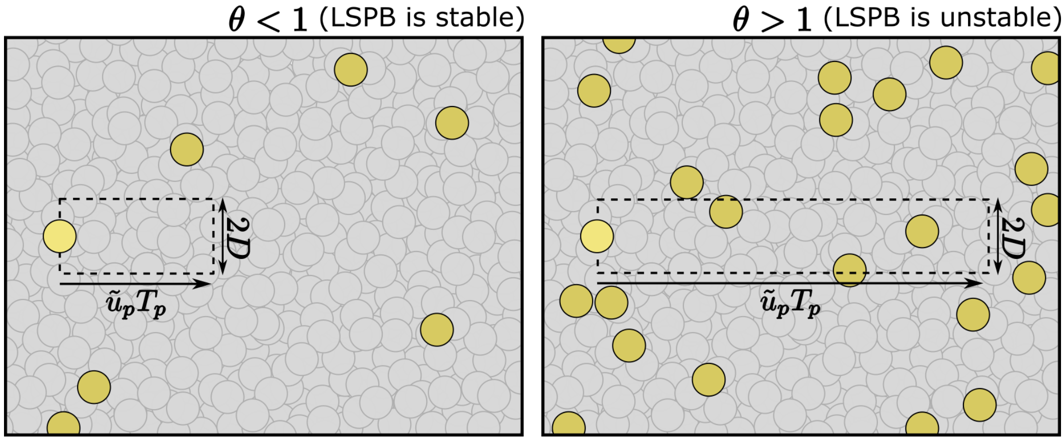

Figure 2. Schematic illustrating rarefied ($\theta < 1$) and congested ($\theta > 1$) transport conditions. Mobile particles are shown in yellow, and immobile particles are shown in grey. A typical particle (light yellow) sweeps out a rectangle with area $2D \times \tilde{u}_p T_p$ during its transit from entrainment to disentrainment. The collision number θ may be interpreted as the average number of particles contained within this rectangle.

two conditions characterized by (a) stable and (b) unstable planar topography, for which we expect to measure θ values below and above 1, respectively.

Experiments were conducted in a 1.19 m wide, 14 m long flume capable of recirculating sediment and water. Flow conditions in the flume could be adjusted by varying (a) the water discharge, (b) the flume slope, and (c) the flow depth at the downstream end. We chose to vary flow conditions by changing the water discharge while holding the outlet flow depth (12 cm) and flume slope (0.001) constant. This allowed for variation in the bed stress while maintaining a constant relative submergence (the ratio of flow depth to grain size). Although this necessarily invokes backwater hydrodynamics, the flow may be treated as quasi-normal because the backwater length $L_{BW} = H/S$ (which characterizes the spatial scale over which flow conditions vary due to backwater effects) was much longer than the length of the test reach. For our experiments, the backwater length was approximately $L_{BW} = O(100)$ m while the test reach was was approximately 2 m.

In order to achieve flow conditions straddling the the threshold of bedform development, we initially allowed topography to equilibrate to a discharge known to produce bedload dominated bedforms (35 L/s). Then, we incrementally reduced the discharge by 5 L/s until planar topography was observed. The bed configuration was allowed to adjust over a period of 24 hours after each reduction in discharge. Using this procedure, we established that plane-bed topography was stable at a water discharge of 20 L/s while bedforms were stable at a water discharge of 25 L/s.

Measurements of flow velocity, bed topography, and particle motion were collected over equilibrium LSPB topography as described in more detail below. Flow velocity was then increased to 25 L/s and identical measurements were immediately made over unstable plane-bed topography. Finally, the bed configuration was allowed to equilibrate to the increased water discharge for roughly 24 hours to verify the presumed instability. Throughout the remainder of this paper, we refer to the stable lower-stage plane bed condition corresponding to 20 L/s water discharge as "SPB", and we refer to the unstable plane-bed condition corresponding to 25 L/s water discharge as "UPB". For clarity, we refer generally to lower-stage plane bed topography as "LSPB".

3.2 Sediment Characteristics and Flow Conditions

The bed material was composed of polystyrene particles with a geometric mean diameter of 2.1 mm and a density of 1.055 g/cm^3. The base-2 logarithmic standard deviation of the grain size distribution was 0.32 (68% of the bed material had a diameter within a factor of $2^{0.32} = 1.24$ of the geometric mean, which is narrower than most naturally-sorted sediments. For this reason, our analyses assume a single grain size sediment equal to the geometric mean grain size. The dimensionless particle Reynolds number ($Re_p = \sqrt{gRD^3}/\nu$, where R is the submerged specific gravity of the sediment, ν is the kinematic viscosity of the fluid, and g is gravitational acceleration) was approximately 70.7, which is equivalent to quartz sand ($R = 1.65$) with diameter $D = 0.68$ mm.

Flow velocity and bed elevation profiles were measured using a Nortek Vectrino Profiler. Shear stress was computed from velocity profiles using a linear fit to the velocity profile (Bagherimiyab & Lemmin, 2013). Shear velocity at 20 L/s water discharge (SPB) computed using this procedure was 0.77 cm/s. Immediately after changing the discharge to 25 L/s (UPB), the ADV-estimated shear velocity was 0.94 cm/s. The dimensionless Shields stresses ($\tau* = u_*^2/gRD$) were 0.052 and 0.077, respectively. The critical Shield's stress for sediment motion estimated from the the formula of Brownlie (1981) is $\tau_{*c} = 0.032$.

Bed elevation profiles were used to quantify variability in bed elevation characteristic of qualitatively planar topography in our experiments. Small surface undulations with slopes well below the angle of repose (maximum 3 degrees) and heights of roughly $H = 3D$ are evident under stable and unstable plane-bed conditions. After the bed was allowed to equilibrate to the 25 L/s water discharge condition, we observed well-developed "3D" dunes (*sensu* Venditti et al., 2005b) with measured lee slopes at the angle of repose (maximum 35 degrees). Bedform height, length, and migration velocity was estimated using crest and trough picking methods from six repeat longitudinal scans covering a distance of 2 m. Measured bedforms had an average height of 2.9 cm, a length of 64 cm, and a migration velocity of 1.4 cm/minute.

3.3 Particle Tracking

Parameters describing the kinematic properties of particle motion were extracted from manually-digitized tracer particle paths. To this end, a small fraction of the bed material was removed from the flume and coated with a thin layer of fluorescent spray paint. These particles were then added back to the flume and allowed to mix with the bed material under a range of flow conditions prior to these experiments. Illuminating the bed with a blacklight increases the contrast of tracer particles relative to other particles so that individual particles can be confidently tracked over long distances. This procedure is also helpful because it reduces the amount of labor required to obtain an unbiased sample of particle motion over a large area and duration.

Tracer particle motions were recorded using a downward facing digital camera attached to a fixed boom 2.05 meters above the water surface. Because the flow velocities needed to mobilize the polystyrene particles were low relative to quartz sand, particles could be tracked through the water surface with a high degree of precision. Videos were rectified and registered using OpenCV (Bradski, 2000) in Python. Manual digitization of particle motions was performed using TrackMate (Tinevez et al., 2017), an open source particle tracking package for ImageJ (Schindelin et al., 2012). In order to minimize sampling bias, all tracer particle motions that occurred within the sampling window during the specified time interval were tracked. Two ten second videos comprising a total of twenty seconds of observations from each experiment were used for this study. After registration, rectification, and trimming, both videos covered a streamwise distance of 230 cm and a cross-stream distance of 108 cm. Analyses reported here were performed using particle motions that occurred within a 30 cm wide, 2 m long control volume in the center

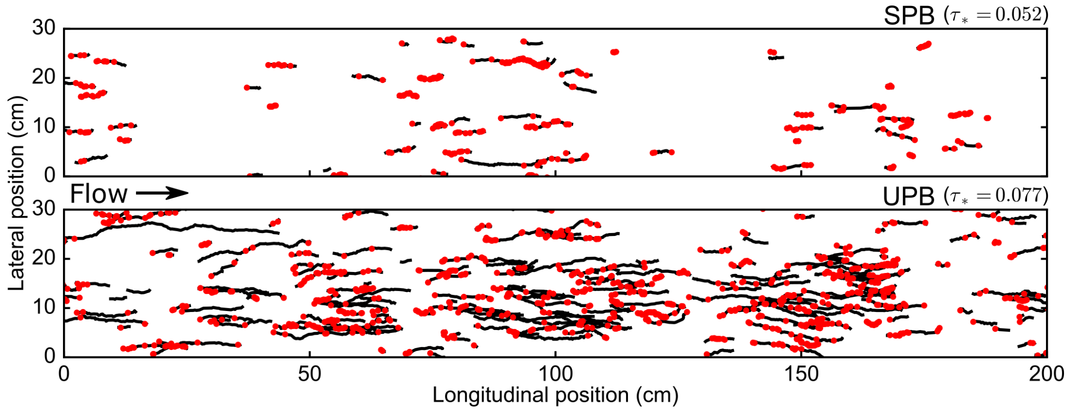

Figure 3. Tracer particle paths (black lines) and entrainment event locations (red dots) for stable lower-stage plane bed and unstable plane bed conditions. Data are from the same total duration for both experiments (20 s) such that apparent differences are representative of the relative sediment loads and entrainment frequencies.

of the flume in order to minimize sidewall effects. Tracked particle paths are plotted in Figure 3.

Particle tracking software records particle location with an arbitrary degree of precision depending on image magnification. Thus, particles which are qualitatively identified as immobile may possess nonzero measured velocities. Furthermore, it is not always clear whether a particle should be considered mobile or immobile. As an example, a resting particle may make several short hops at high velocities separated by only a few frames where the velocity is near-zero; it is unclear whether these should be treated as one or several hops. Following previous studies (e.g., Lajeunesse et al., 2010; Liu et al., 2019; Ashley, Mahon, et al., 2020), we employed a velocity threshold criteria to distinguish mobile and immobile particles. Velocity thresholds provide a robust, reproducible solution to this problem. Recognizing that the motion state of certain particles is unclear, we inspected motions identified using a range of velocity thresholds and found that values between $u_c = 0.005$ m/s to $u_c = 0.01$ m/s differentiated between mobile and immobile particles in a manner that is consistent with visual identification. Below 0.005 m/s, particles which remain in the same location for significant durations are identified as mobile, and above 0.01 m/s, particles which are clearly in motion in the bedload phase are identified as immobile. The exact values of certain computed quantities are sensitive to the specific choice of velocity threshold within this range, however the primary findings of this work are not. Detailed sensitivity analysis was performed using velocity thresholds ranging from 0.0001 m/s to 0.1 m/s and is discussed in detail in Section 6.2. Reported results were obtained using a velocity threshold of 0.007 m/s, which is approximately the geometric midpoint of the optimum range (0.005 m/s to 0.01 m/s).

In order to estimate certain bulk statistics of sediment transport from tracer particle statistics, it was necessary to estimate the tracer fraction in the flume. This was accomplished by collecting a sample of the bed material from three locations dispersed across the bed after the experimental campaign was complete. The total mass of the sample was 760 g. Tracer particles were separated by hand under a blacklight and then weighed. The total mass of tracer particles in the sample was 1.49 g. Thus, we estimate the tracer fraction to be 0.00196.

4 Methods for Computing Particle Motion Statistics From Digitized Particle Paths

4.1 Particle Position and Velocity

The kinematic statistics of particle motion needed to estimate θ using equation (3) were computed from digitized particle paths following Ballio et al. (2018). We consider digitized particle motions within a 2.0 m long by 0.3 m wide control volume extending from the flume bottom to the water surface are projected onto a 2 dimensional plane A (Figure 3). Each particle motion is defined by a sequence of discrete measurements of particle position on the domain of longitudinal position x, and lateral position y. The position of the i^{th} of m tracked particles in the j^{th} of n frames is expressed by the vector $\mathbf{x}_{i,j}$ with longitudinal and lateral components $x_{i,j}$ and $y_{i,j}$.

Particle velocities are computed by comparing subsequent positions of a particle. Measured velocities therefore represent temporal averages between the two measurements of particle position; however, the time between frames δt is sufficiently small that it may be viewed as an instantaneous velocity for the purpose of differentiating between mobile and immobile particles. The velocity vector $\mathbf{u}_{i,j}$ with longitudinal and lateral components $u_{i,j}$ and $v_{i,j}$ is computed as

$$\mathbf{u}_{i,j} = \frac{\mathbf{x}_{i,j+1} - \mathbf{x}_{i,j}}{\delta t}. \tag{6}$$

4.2 Mean Granular Activity γ_g

We focus primarily on count-based descriptions of particle motion which pertain directly to the estimation of θ as opposed to volumetric quantities like the volumetric activity γ (L) and the volumetric entrainment rate E (L/T). Count-based (granular) quantities are denoted by the subscript g.

The mean granular activity is computed by counting the number of active tracer particles in the control volume in each frame and averaging. This is accomplished using an Eulerian clipping function M^A to quantify whether the i^{th} tracer particle is within the control area A in the j^{th} frame:

$$M^A_{i,j} = \begin{cases} 1, & \text{if } \mathbf{x}_{i,j} \in A \\ 0, & \text{otherwise} \end{cases}. \tag{7}$$

Additionally, a velocity threshold u_c is used to define the state of motion of a particle quantified by the clipping function M^m:

$$M^m_{i,j} = \begin{cases} 1, & \text{if } ||\mathbf{u}_{i,j}|| \geq u_c \\ 0, & \text{otherwise} \end{cases} \tag{8}$$

where $||\mathbf{u}_{i,j}||$ is the particle speed. Thus, the number of mobile tracer particles in the control volume in frame j is given by:

$$N^{m,A}_j = \sum_{i=1}^{m} M^m_{i,j} M^A_{i,j}. \tag{9}$$

Tracer particle positions recorded in n frames lead to $n-1$ measurements of velocity, and the average number of moving tracer particles within the control volume over all frames with valid velocity measurements is given by:

$$\langle N^{m,A} \rangle = \frac{1}{n-1} \sum_{j=1}^{n-1} N^{m,A}_j. \tag{10}$$

Here, angle brackets denote sample averages which we assume provide unbiased estimates of the ensemble average.

The granular activity is estimated by dividing $\langle N^{m,A}\rangle$ by the tracer particle fraction ψ and the control volume area:

$$\gamma_g = \frac{\langle N^{m,A}\rangle}{\psi A}. \tag{11}$$

Note that γ_g is an an estimate of a mean, but angle brackets are dropped to simplify notation in Section 2.

4.3 Mean Deviatoric Speed $\tilde{u}_p$

In order to estimate the mean deviatoric speed, it is first necessary to compute the mean particle velocity vector. The mean velocity of moving tracer particles in the control volume is given by

$$\langle \mathbf{u}^{m,A}\rangle = \frac{1}{(n-1)\langle N^{m,a}\rangle}\sum_{i=1}^{m}\sum_{j=1}^{n}\mathbf{u}_{i,j}M^m_{i,j}M^A_{i,j} \tag{12}$$

where $(n-1)\langle N^{m,a}\rangle$ is the total number of measurements of tracer particle speed that exceed the threshold speed. The mean deviatoric speed of tracer particles is then estimated as

$$\langle \tilde{u}^{m,A}\rangle = \frac{1}{(n-1)\langle N^{m,a}\rangle}\sum_{i=1}^{m}\sum_{j=1}^{n}||\mathbf{u}_{i,j} - \langle \mathbf{u}^{m,A}\rangle||M^m_{i,j}M^A_{i,j} \tag{13}$$

We assume that the average deviatoric speed of tracer particles in the control volume is equivalent to the average deviatoric speed of all mobile particles characteristic of macroscopic flow conditions, that is,

$$\tilde{u}_p = \langle \tilde{u}^{m,A}\rangle. \tag{14}$$

Again, this quantity is an estimate of a mean; however, angle brackets are dropped to simplify notation in Section 2.

The mean longitudinal particle velocity u_x can be estimated by substituting $u_{i,j}$ for $\mathbf{u}_{i,j}$ in equation (12). Once the granular activity γ_g and mean longitudinal velocity u_x are known, the ensemble average granular particle flux characteristic of macroscopic flow conditions q_{sg} ($\mathrm{L}^{-1}\mathrm{T}^{-1}$) may be estimated as $q_{sg} = \gamma_g u_x$.

4.4 Granular Entrainment Frequency E_g

The final relevant quantity that must be estimated to compute θ with equation (3) is the entrainment frequency E_g. Entrainment and disentrainment events are defined as transitions between the mobile and immobile states and are quantified by differentiating M^m with respect to time (Ballio et al., 2018). Presently, we define an entrainment function M^E as

$$M^E_{i,j} = M^m_{i,j} - M^m_{i,j-1}. \tag{15}$$

This function may take on values of 1, 0, or −1, signifying an entrainment event, no event, or a disentrainment event. Assuming the spatially-averaged time rate of change of bed elevation is zero within and around the control volume, the entrainment frequency E_g and the disentrainment frequency D_g must be equal. Consequently, the spatially averaged entrainment and disentrainment frequencies can be estimated from the absolute value of M^E as

$$E_g = D_g = \frac{1}{(n-2)\delta t}\sum_{i=1}^{m}\sum_{j=2}^{n-1}\frac{1}{2}|M^E_{i,j}|M^A_{i,j}. \tag{16}$$

Here, $(n-2)\delta t$ is the total time over which it is possible to detect entrainment events occurring in n frames.

Table 1. Summary of Experiments

	SPB	UPB
Boundary Conditions		
Geometric mean particle diameter D	2.1 mm	2.1 mm
Sediment density ρ_s	1.055 g/cm^3	1.055 g/cm^3
Particle Reynolds Number Re_p	70.7	70.7
Unit water discharge q_w	0.016 m^2/s	0.021 m^2/s
Flow depth in test area h	0.11 m	0.11 m
ADV Shear velocity u_*	0.0077 m/s	0.0094 m/s
Shields stress τ_*	0.052	0.077
Results		
Granular activity γ_g	3800 m^{-2}	20,300 m^{-2}
Mean deviatoric speed $\tilde{u}_p$	3.6 cm/s	4.1 cm/s
Mean longitudinal velocity u_x	2.8 cm/s	3.3 cm/s
Entrainment frequency E_g	15400 m^{-2}s^{-1}	43300 m^{-2}s^{-1}
Mean travel time τ	0.25 s	0.47 s
Granular sediment flux q_{sg}	106 m^{-1}s^{-1}	668 m^{-1}s^{-1}
Volumetric sediment flux q_s	5.15 $\times 10^{-7}$ m^2/s	3.24 $\times 10^{-6}$ m^2/s
Einstein bedload number q_*	0.0073	0.046
Mean free path λ	6.3 cm	1.2 cm
Characteristic transport length $\tilde{u}_p\tau$	0.9 cm	1.9 cm
Collision number θ	**0.14**	**1.65**

5 Results

For the SPB condition, the experimental procedure described above yielded a total of 2685 measurements of particle speed in excess of the threshold speed in the control volume belonging to 65 unique particles (Figure 3). The entrainment function (equation 15) was used to identify a total of 725 tracer particle exchanges with the bed (entrainment and disentrainment events). The ensemble average tracer particle flux was 0.21 particles per second per meter width. This leads to a total granular flux $q_{sg} = 106$ particles per second per meter width and a dimensionless bedload flux $q_* = q_g V_p/\sqrt{RgD^3}$ of 0.0073. Solving the Wong and Parker (2006) bedload equation for shear velocity using the critical Shields stress predicted from Brownlie (1981) leads to $u_* = 0.0073$ m/s compared with 0.0077 m/s estimated using acoustics.

For the UPB condition, experiments produced 14309 measurements of mobile particles in the control volume belonging to 231 unique particles (Figure 3). The entrainment function identified 2032 exchanges with the bed. The ensemble average tracer particle flux was 1.3 particles per second per meter width leading to a total granular flux of $q_{sg} = 668$ particles per second per meter width and a dimensionless bedload number of $q_* = 0.045$. The shear velocity estimated from q_* was $u_* = 0.0097$ m/s compared with 0.0094 m/s estimated using acoustics.

Experimental results are reported in Table 5. Notably, the collision number varies by over an order of magnitude between the two experiments from 0.14 to 1.65. In terms of the Knudsen number interpretation of θ, the observed difference reflects both an increase in the characteristic length $\tilde{u}_p\tau$ and a decrease in the mean free path λ.

6 Discussion

For the experimental conditions considered here, we find that the transition from LSPB to bedforms corresponds to the transition from rarefied to congested sediment transport conditions parameterized by the collision number θ. Despite only a small increase in shear stress, θ increases by over a factor of 10, from 0.14 for the SPB condition to 1.65 for the UPB condition. Our results demonstrate that a careful interpretation of observations made by previous authors (e.g., Coleman & Nikora, 2011) leads to a quantitative prediction that is consistent with measurements, supporting a hypothesized causal link between particle collisions and bedform development.

Here, we consider the theoretical implications of this finding by reexamining the arguments used to justify our hypothesis. In Section 1, we argued that well-developed ripples and dunes are distinct from microforms like bedload sheets, particle clusters, and low-amplitude ripples and dunes due to a transition in process regime and scaling. Three mechanisms are invoked to explain this transition, each of which represents a coherent synthesis of previous observations and theory. We emphasize that these mechanisms are not evaluated independently, but are considered here because they provide a mechanical explanation of our results and a starting point for future studies.

First, we suggest that microforms are an inevitable outcome of fluid driven sediment transport. This follows from the notion that quasi-random motions of particles produce grain-scale disturbances in bed elevation. The formation of grain-scale disturbances driven by turbulent fluid flow has been described by a number of authors (Williams & Kemp, 1971; Best, 1992); Whiting and Dietrich (1990) and Clifford et al. (1992) argue that the difference between fixed- and mobile- bed roughness is explained by this phenomenon. More generally, we suggest that microforms are a manifestation of inevitable self-organization of granular bed disturbances through inelastic particle collisions (Shinbrot, 1997).

Second, we suggest that microform amplitude scales with particle diameter and collision frequency. Coleman and Nikora (2009, 2011) argued that interactions between mobile clusters of particles increase the size of disturbances in bed elevation. This implies that there is a balance between disturbance growth and decay, where growth is related to particle collisions and decay is related to disturbance size, perhaps due to the fact that particles are more likely to be eroded from topographic highs and deposited in topographic lows. We suggest that the stable microform amplitude H_μ is related to the collision number, for example as $H_\mu/D \propto \theta$.

Finally, we suggest that microforms are stable up to a critical amplitude, above which flow separation and scour at the point of reattachment cause nonlinear pattern coarsening. Studies that describe bedform growth from artificial or natural defects typically find that small defects are suppressed rather than amplified (Southard & Dingler, 1971; Gyr & Schmid, 1989; Gyr & Kinzelbach, 2004; Venditti et al., 2005a; Coleman & Nikora, 2009). Only when defects exceed a critical height, usually reported as a constant multiple of particle diameter ranging from 2-4, do they stabilize and propagate (Williams & Kemp, 1971; Leeder, 1980; Costello & Southard, 1981; Coleman & Nikora, 2009, 2011). This transition in process regime fundamentally distinguishes quasi-planar configurations from well-developed ripples and dunes.

6.1 Implications for Stability Diagrams

Here, we demonstrate that our results are consistent with empirical stability fields proposed based on observations of topographic configuration under a wide range of conditions (e.g., Van den Berg & Van Gelder, 1993; Southard & Boguchwal, 1990; Carling, 1999; García, 2008). This is accomplished by combining existing theoretical and empirical relations to obtain an expression for θ in terms of macroscopic boundary conditions.

Specifically, we derive an expression of the form

$$\theta = f(\tau_*, Re_p), \tag{17}$$

such that the threshold of bedform development can be represented as $f(\tau_*, Re_p) = 1$. Starting with equation 5, this expression may be obtained by invoking four relations outlined here and discussed in more detail below. These are (a) an expression relating the mean longitudinal particle velocity to the mean deviatoric particle speed, (b) a kinematic description of the volumetric flux in terms of the mean longitudinal velocity, the granular particle activity, and the particle volume (c) an empirical relation for the mean particle travel time, and (d) an empirical bedload transport formula.

The first element (a) is necessary because the mean deviatoric particle speed is a relatively obscure quantity that is not referenced in existing literature. In contrast, the mean longitudinal velocity is an essential component of the flux and is relatively well-studied (Lajeunesse et al., 2010, references therein). These quantities may be related by assuming a joint probability distribution model for longitudinal and lateral particle velocity. Several authors have proposed functional forms for the margins of this distribution (e.g., Furbish & Schmeeckle, 2013; Fathel et al., 2015; Furbish et al., 2016; Liu et al., 2019), however the correlation behavior and relative magnitudes of longitudinal and lateral components are not well-constrained, precluding the possibility of a purely theoretical derivation. Instead, we assume

$$\tilde{u}_p = \alpha u_x, \tag{18}$$

where α is a coefficient of order unity. Neglecting lateral velocities and assuming longitudinal velocities are exponentially distributed leads to $\alpha = 2/e \approx 0.73$. This may be interpreted as a lower bound because upstream motions and nonzero lateral velocities will increase the mean deviatoric speed relative to the mean longitudinal speed. We find that $\alpha = 1.28$ for the SPB condition and $\alpha = 1.26$ for the UPB condition. For simplicity, we assume a fixed value of $\alpha = 5/4$.

The second element (b) is an exact expression for the average bedload flux q_b under steady, uniform macroscopic transport conditions (Furbish et al., 2012) given by

$$q_b = \gamma u_x. \tag{19}$$

Here, we point out that this expression may be combined with (18), and substituted into (5) to obtain:

$$\theta = \frac{12\alpha q_b T_p}{\pi D^2}. \tag{20}$$

noting that $\gamma = \gamma_g V_p$, where V_p is a characteristic particle volume taken to be the volume of a sphere with diameter D.

The third element (c) is an empirical relation for the mean particle travel time T_p. This is perhaps the most uncertain element in predicting θ, owing in part to experimental censorship and discrepancies in the strategies employed in different studies to delineate mobile and immobile particles (Hosseini-Sadabadi et al., 2019). Lajeunesse et al. (2010) reviewed previous work and concluded based on physical and dimensional arguments that the mean travel should be predicted as

$$T_p = \beta \frac{D}{\omega_s}\left(\frac{u_* - u_{*c}}{\omega_s}\right)^{\varepsilon} \tag{21}$$

where ω_s is the particle settling velocity, u_* is the shear velocity, u_{*c} is the critical shear velocity for sediment motion, and β and ε are empirical coefficients. Based on available data, they suggest that that $\beta = 10.7$ and $\varepsilon = 0$, removing the dependence on shear velocity. The settling velocity may be expressed by $\omega_s = \sqrt{4RgD/3C_d}$, where C_d is a

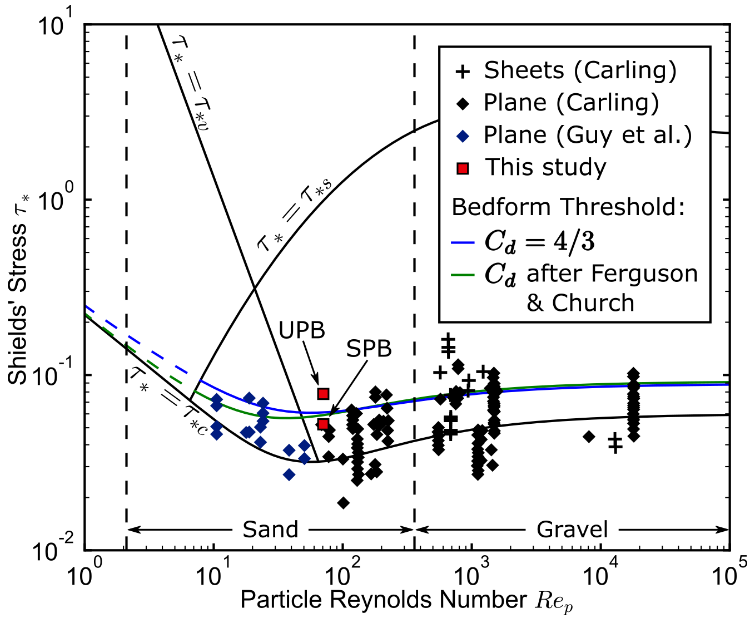

Figure 4. Shields-Parker river sedimentation diagram with theoretical microform-mesoform transition (Equation 24) for two particle settling models. Dashed segment indicates the region where model assumptions are not expected to hold due to significant suspension. As expected, the SPB condition plots below the threshold while the UPB condition plots above the threshold. The observations of planar topography and bedload sheets reported by Carling (1999) are plotted in for comparison. Also plotted are observations of planar topography reported by Guy et al. (1966) that were ignored by Southard and Boguchwal (1990) and Van den Berg and Van Gelder (1993) in delineating classic stability fields.

drag coefficient. Combining equations (20) and (21) with suggested values for α and β leads to

$$\theta = 44.2\sqrt{C_d}q_* \tag{22}$$

where $q_* = q_b/\sqrt{gRD^3}$ is the Einstein bedload number.

The final component (d) is the empirical bedload transport equation of Wong and Parker (2006) given by

$$q_* = 3.97(\tau_* - \tau_{*c})^{3/2}. \tag{23}$$

Substituting this expression into (22) and setting $\theta = 1$ provides a prediction of the threshold Shields stress for bedform development $\tau_{*\theta}$ corresponding to the transition from rarefied to congested transport:

$$\tau_{*\theta} = \left(\frac{0.0057}{\sqrt{C_d}}\right)^{2/3} + \tau_{*c} \tag{24}$$

where $\tau_{*c} = f(Re_p)$ after Brownlie (1981) and $C_d = f(Re_p)$ after Ferguson and Church (2004). We also note that neglecting viscous settling, $C_d \approx 4/3$ following Lajeunesse et al. (2010) results in almost no change in the stability field for LSPB topography (Figure 4). Similarly, nonzero values of ε will shift the value of $\tau_{*\theta}$ up or down slightly without significantly altering the shape or qualitative fit to existing data.

The stability field for LSPB topography implied by this expression is plotted in Figure 4. We find that the theoretical prediction is aligned with observational data compiled by Carling (1999). This figure also includes observations of planar topography reported by Guy et al. (1966) that were ignored in subsequent stability diagrams because they are within the hydraulically smooth regime. (Southard & Boguchwal, 1990) asserted that these conditions would have eventually produced ripples, however we suggest that the relief of stable ripples would be small leading to poorly-developed flow separation. As a result, they could be considered quasi-planar microforms by the criteria proposed above.

We note here that the empirical stability fields for planar topography and bedforms overlap substantially, with many observations of bedforms occurring in the region where $\theta < 1$. We offer several possible explanations. First, low-amplitude bedforms with poorly developed flow separation could potentially appear qualitatively similar to ripples and dunes in planform. In this case, they might be labeled as bedforms while being more appropriately classified as microforms in the context of the present research. Second, there is substantial variability in methodology used to compute the Shields' stress across different studies, and uncertainty is large for low values near the threshold of motion. Third, the observed overlap may be a genuine feature of the data. If this is true, it implies that either (a) the method for estimating θ as a function of tau_* and Re_p is incomplete, or (b) $\theta = 1$ merely provides an upper limit for plane-bed stability. In either case, the bed configuration likely depends on an additional parameter not considered here like the slope or the Froude number.

6.2 Sensitivity of Results to the Choice of Mobility Threshold u_c

Sensitivity analysis was performed to determine whether results are sensitive to the value of u_c, the cutoff value for particle velocity used to identify mobile particles (equation 8). All quantities were computed using 20 logarithmically spaced values for u_c ranging from 0.001 m/s to 0.1 m/s. Select results are plotted in Figure (5).

The main objective of this exercise is to determine whether small changes in u_c influence our conclusions regarding θ. While the values of θ are sensitive to u_c, we find that the the value for the UPB condition exceeds the value for the SPB condition by over an order of magnitude across the full range of u_c values tested (Figure 5A). We also find the value for the UPB condition exceeds 1 while the value for the SPB condition is less than 1 for reasonable values of u_c identified by inspecting particle motions. Above $u_c \approx$ 0.15 m/s, we find $\theta < 1$ for the UPB experiment, however this result is unrealistic because clearly mobile particles are ignored. Furthermore, $\theta = \mathrm{O}(1)$ up to $u_c \approx 0.03$ for UPB, compared with SPB, for which $\theta = \mathrm{O}(0.1)$. While results obtained using 0.015 m/s $< u_c <$ 0.03 m/s independelty are equivocal, we argue that the behavior of θ as a function of u_c is expected and holistically supports the hypothesis and interpretations discussed above.

Estimates of tracer particle flux, total granular flux, and volumetric flux (which are related by the tracer fraction and nominal particle volume) are also not sensitive to u_c across the optimum range. However, computed sediment load decreases rapidly for $u_c >$ 0.02 m/s because particles that contribute significantly to the measured sediment load are ignored (Figure 5B). This observation provides a quantitative upper bound for u_c and supports the notion that θ values computed above this bound are unreasonable. In contrast, arbitrarily low values of u_c provide consistent estimates of flux. This is also expected; recall that the flux is calculated as $q_b = \gamma_g u_x$. Including immobile particles with near-zero velocities in the calculation of sediment load increases γ_g but decreases u_x by reciprocal factors such that there is no change in estimates of q_b.

Other relevant quantities (for example, entrainment rates, activities, velocities) are sensitive to the choice of velocity threshold. Computed quantities typically vary slowly as monotonic functions of u_c up to the point where u_c is a significant fraction of the maximum measured particle speed (roughly $u_c = 0.02$ m/s in our experiments). Above this threshold, computed quantities vary rapidly with u_c as mobile particles are increasingly ignored. The average particle speed (the magnitude of the velocity vector) exemplifies this behavior (Figure 5C). Interestingly, we find that the difference between the mean computed particle speed and the threshold speed ($u_p - u_c$) is maximized across the optimum range of velocity values that was determined independently by inspecting particle motions. Below this range, immobile particles included in the computation of mean velocity cause a decrease in the excess particle speed; above, the threshold speed begins to approach the maximum measured particle speed. This observation potentially provides an objective approach for selecting a velocity threshold.

7 Conclusions

This study clarifies the nature of lower-stage plane bed topography and the granular mechanics of ripple and dune initiation. As a starting point, we recognize that the concept of planar topography breaks down at the granular scale and propose a definition of lower-stage plane bed topography that encompasses microforms like bedload sheets, particle clusters, and other low-amplitude bedforms. This definition is appropriate because it is aligned with a hypothesized transition in process regime corresponding to the onset of defect propagation and nonlinear coarsening. It is also aligned with practical considerations related to form roughness, drag partitioning, and preserved sedimentary structures.

Previous studies suggest that particle collisions are important during the initial phase of bedform development. We formalize this idea to propose a quantitative hypothesis that is tested using experimental observations of tracer particle motion over stable and unstable planar topography. Specifically, we hypothesize that quasi-planar topography becomes unstable when the particle collision frequency exceeds the particle entrainment frequency. The dimensionless ratio of these quantities, called the "collision number", is like an inverse Knudsen number commonly used in fluid physics to quantify the transition from rarefied to continuum transport. We find that the collision number is 0.14 in the stable plane bed condition and 1.65 in the unstable plane bed condition despite only a small increase in bed stress, supporting our hypothesis.

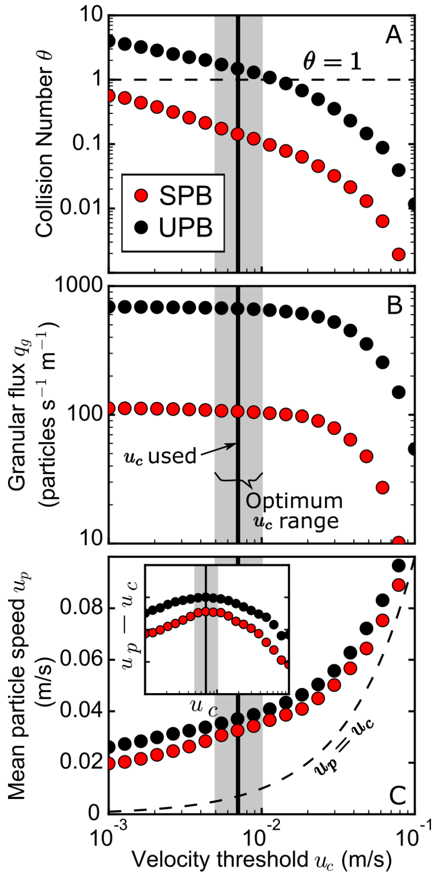

Figure 5. Plot illustrating the effect of the velocity threshold u_c on the measured variables. Although θ is sensitive to the choice of velocity threshold, it varies by an order of magnitude regardless of the specific value used (A). Additionally, measured values straddle $\theta = 1$ within the optimum u_c range. Sediment load is not sensitive to u_c except at very large values because particles that meaningfully contribute to the measured sediment load are ignored (B). We find that the optimum u_c range determined by inspection (Section 6.2) corresponds to the maximum difference between the mean measured particle speed and u_c (C).

Combining empirical and theoretical expressions enables prediction of the collision number (and as a result, bed configuration) as a function of macroscopic boundary conditions. We find that the predicted stability field for microforms is consistent with observations of lower-stage plane bed topography and bedload sheets reported by Carling (1999) and Guy et al. (1966). Although ripples and dunes have been observed in the region where the collision number is predicted to be less than 1, this may be explained by misclassification of low-amplitude bedforms or uncertainty in measurements of stress. If the overlap is genuine, bed configuration may exhibit weak dependence on an additional parameter like slope or Froude number.

In summary, our primary hypotheses represents a coherent synthesis of existing process-based descriptions of bedform initiation focused on various elements of turbulent fluid flow, grain-scale transport, and topographic change. It is supported by experiments reported here and observations of bed configuration reported by previous authors. Three mechanisms are proposed to explain this finding. First, we suggest that grain-scale bed disturbances inevitably self-organize into microforms like bedload sheets, particle clusters, and other low-amplitude bedforms. Second, we suggest that microform amplitude scales with particle diameter and collision frequency. Finally, we suggest that defect propagation and nonlinear coarsening occurs when microform height exceeds a critical height that is a constant multiple of particle diameter. These mechanisms provide a possible explanation for our results and a starting point for future studies that aim to investigate the mechanisms that determine the stable bed configuration under weak bedload transport conditions.

Acknowledgments

We thank the donors of the American Chemical Society Petroleum Research Fund 54492-DNI8, the National Science Foundation (NSF) grant EAR-1632938, and the University of Wyoming School of Energy Resources for partially supporting this research. We also thank Jelle ten Harkel, Noortje Oosterhoff, and Avelon Gerritsma for assistance with experiments and particle tracking. Data and code are available through Figshare (Ashley, Naqshband, & McElroy, 2020)

References

Ashley, T. C., Mahon, R. C., Naqshband, S., Leary, K. C. P., & McElroy, B. J. (2020). Probability distributions of particle hop distance and travel time over equilibrium mobile bedforms. *Journal of Geophysical Research: Earth Surface*.

Ashley, T. C., Naqshband, S., & McElroy, B. J. (2020). Data and code for "Particle collisions control stable bed configuration under weak bedload transport conditions". *Figshare Dataset*. doi: https://doi.org/10.6084/m9.figshare.12475865.v1

Baas, J. H., Best, J. L., & Peakall, J. (2016). Predicting bedforms and primary current stratification in cohesive mixtures of mud and sand. *Journal of the Geological Society*, *173*(1), 12–45. doi: 10.1144/jgs2015-024

Bagherimiyab, F., & Lemmin, U. (2013). Shear velocity estimates in rough-bed open-channel flow. *Earth Surface Processes and Landforms*, *38*(14), 1714–1724. doi: 10.1002/esp.3421

Bagnold, R. A. (1935). The movement of desert sand. *Proceedings of the Royal Society of London. Series A - Mathematical and Physical Sciences*, *157*(892), 594–620. doi: 10.1098/rspa.1936.0218

Ballio, F., Pokrajac, D., Radice, A., & Hosseini Sadabadi, S. A. (2018). Lagrangian and Eulerian description of bed load ransport. *Journal of Geophysical Research: Earth Surface*, *123*(2), 384–408. doi: 10.1002/2016JF004087

Best, J. L. (1992). On the entrainment of sediment and initiation of bed defects: insights from recent developments within turbulent boundary layer research. *Sed-*

imentology, *39*(5), 797–811. doi: 10.1111/j.1365-3091.1992.tb02154.x

Best, J. L. (1996). The fluid dynamics of small-scale alluvial bedforms. In P. A. Carling & M. R. Dawson (Eds.), *Advances in fluvial dynamics and stratigraphy* (pp. 67–125). Manchester, United Kingdom: John Wiley and Sons.

Best, J. L. (2005). The fluid dynamics of river dunes: A review and some future research directions. *Journal of Geophysical Research: Earth Surface*, *110*(F4). doi: 10.1029/2004JF000218

Bialik, R. J. (2011). Particle-particle collision in Lagrangian modelling of saltating grains. *Journal of Hydraulic Research*, *49*(1), 23–31. doi: 10.1080/00221686.2010.543778

Bradski, G. (2000). The OpenCV library. *Dr. Dobb's Journal of Software Tools*, *25*.

Brownlie, W. R. (1981). *Prediction of flow depth and sediment discharge in open channels* (Tech. Rep. No. 43A). Pasadena, California: W. M. Keck Laboratory of Hydraulics and Water Resources, California Institute of Technology.

Carling, P. A. (1999). Subaqueous gravel dunes. *Journal of Sedimentary Research*, *69*(3), 534–545. doi: 10.2110/jsr.69.534

Carling, P. A., Richardson, K., & Ikeda, H. (2005). A flume experiment on the development of subaqueous fine-gravel dunes from a lower-stage plane bed. *Journal of Geophysical Research: Earth Surface*, *110*(F4). doi: 10.1029/2004JF000205

Charru, F., Andreotti, B., & Claudin, P. (2013). Sand ripples and dunes. *Annual Review of Fluid Mechanics*, *45*(1), 469–493. doi: 10.1146/annurev-fluid-011212-140806

Clifford, N. J., Robert, A., & Richards, K. S. (1992). Estimation of flow resistance in gravel-bedded rivers: A physical explanation of the multiplier of roughness length. *Earth Surface Processes and Landforms*, *17*(2), 111–126. doi: 10.1002/esp.3290170202

Coleman, S. E., & Eling, B. (2000). Sand wavelets in laminar open-channel flows. *Journal of Hydraulic Research*, *38*(5), 331–338. doi: 10.1080/00221680009498314

Coleman, S. E., & Melville, B. W. (1994). Bed-form development. *Journal of Hydraulic Engineering*, *120*(5), 544–560. doi: 10.1061/(ASCE)0733-9429(1994)120:5(544)

Coleman, S. E., & Melville, B. W. (1996). Initiation of bed forms on a flat sand bed. *Journal of Hydraulic Engineering*, *122*(6), 301–309. doi: 10.1061/(asce)0733-9429(1996)122:6(301)

Coleman, S. E., & Nikora, V. I. (2009). Bed and flow dynamics leading to sediment-wave initiation. *Water Resources Research*, *45*(4), 1–12. doi: 10.1029/2007WR006741

Coleman, S. E., & Nikora, V. I. (2011). Fluvial dunes: Initiation, characterization, flow structure. *Earth Surface Processes and Landforms*, *36*(1), 39–57. doi: 10.1002/esp.2096

Costello, W. R. (1974). *Development of bed configurations in coarse sands* (Ph.D. Dissertation). Massachusetts Institute of Technology.

Costello, W. R., & Southard, J. B. (1981). Flume experiments on lower-flow-regime bed forms in coarse sand. *SEPM Journal of Sedimentary Research*, *51*(3), 849–864. doi: 10.1306/212F7DC4-2B24-11D7-8648000102C1865D

Dade, W. B., & Friend, P. F. (1998). Grain size, sediment-transport regime and channel slope in alluvial rivers. *Journal of Geology*, *106*(6), 661–675.

Dunne, K. B., & Jerolmack, D. J. (2018). Evidence of, and a proposed explanation for, bimodal transport states in alluvial rivers. *Earth Surface Dynamics*, *6*, 583–594. doi: 10.5194/esurf-6-583-2018

Eaton, B. C., Church, M., & Millar, R. G. (2004). Rational regime model of alluvial channel morphology and response. *Earth Surface Processes and Landforms*, *29*(4), 511–529. doi: 10.1002/esp.1062

Einstein, H. A. (1950). The bed-load function for sediment transportation in open channel flows. *U.S. Department of Agriculture Technical Bulletin 1026*.

Engelund, F., & Fredsoe, J. (1982). Sediment ripples and dunes. *Annual Review of Fluid Mechanics*, *14*(1), 13–37. doi: 10.1146/annurev.fl.14.010182.000305

Engelund, F., & Hansen, E. (1967). *A monograph on sediment transport in alluvial streams* (Tech. Rep.). Technical University of Denmark. doi: 10.1007/s13398-014-0173-7.2

Fathel, S., Furbish, D. J., & Schmeeckle, M. W. (2015). Experimental evidence of statistical ensemble behavior in bed load sediment transport. *Journal of Geophysical Research: Earth Surface*, *120*(11), 2298–2317. doi: 10.1002/2015JF003552

Ferguson, R. I., & Church, M. (2004). A simple universal equation for grain settling velocity. *Journal of Sedimentary Research*, *74*(6), 933–937. doi: 10.1306/051204740933

Fredsoe, J. (1982). Shape and dimensions of stationary dunes in rivers. *Journal of the Hydraulics Division of the American Society of Civil Engineers*, *108*(8), 932–947.

Furbish, D. J. (1997). *Fluid physics in geology: An introduction to fluid motions on Earth's surface and within its crust.* New York: Oxford University Press.

Furbish, D. J., Fathel, S. L., Schmeeckle, M. W., Jerolmack, D. J., & Schumer, R. (2017). The elements and richness of particle diffusion during sediment transport at small timescales. *Earth Surface Processes and Landforms*, *42*(1), 214–237. doi: 10.1002/esp.4084

Furbish, D. J., Haff, P. K., Roseberry, J. C., & Schmeeckle, M. W. (2012). A probabilistic description of the bed load sediment flux: 1. Theory. *Journal of Geophysical Research: Earth Surface*, *117*(F3). doi: 10.1029/2012JF002352

Furbish, D. J., & Schmeeckle, M. W. (2013). A probabilistic derivation of the exponential-like distribution of bed load particle velocities. *Water Resources Research*, *49*(3), 1537–1551. doi: 10.1002/wrcr.20074

Furbish, D. J., Schmeeckle, M. W., Schumer, R., & Fathel, S. L. (2016). Probability distributions of bed load particle velocities, accelerations, hop distances, and travel times informed by Jaynes's principle of maximum entropy. *Journal of Geophysical Research: Earth Surface*, *121*(7), 1373–1390. doi: 10.1002/2016JF003833

García, M. H. (2008). Sediment transport and morphodynamics. In *Sedimentation engineering* (pp. 21–163). Reston, VA: American Society of Civil Engineers. doi: 10.1061/9780784408148.ch02

Gomez, B., Naff, R. L., & Hubbell, D. W. (1989). Temporal variations in bedload transport rates associated with the migration of bedforms. *Earth Surface Processes and Landforms*, *14*(2), 135–156. doi: 10.1002/esp.3290140205

Guy, H., Simons, D. B., & Richardson, E. (1966). Summary of alluvial channel data from flume experiments, 1956-61. *U.S. Geology Survey Professional Paper 462-I*.

Gyr, A., & Kinzelbach, W. (2004). Bed forms in turbulent channel flow. *Applied Mechanics Reviews*, *57*(1), 77–93. doi: 10.1115/1.1584063

Gyr, A., & Schmid, A. (1989). The different ripple formation mechanisms. *Journal of Hydraulic Research*, *27*(1), 61–74. doi: 10.1080/00221688909499244

Hosseini-Sadabadi, S. A., Radice, A., & Ballio, F. (2019). On reasons of the scatter of literature data for bed-load particle hops. *Water Resources Research*, *55*(2), 1698–1706. doi: 10.1029/2018WR023350

Hubbell, D. W., Stevens, H. H., Skinner, J. V., & Beverage, J. P. (1987). Laboratory data on coarse- sediment transport for bedload-sampler calibrations. *U.S. Geological Survey Water-Supply Paper 2299*.

Ikeda, H. (1983). Experiments on bedload transport, bedforms, and sedimentary structures using fine gravel in the 4-meter-wide flume. *Environmental Research*

Center Papers, Environmental Research Center, University of Tsukuba, *2*, 1–78.

Ikeda, S., Parker, G., & Kimura, Y. (1988). Stable width and depth of straight gravel rivers with heterogeneous bed materials. *Water Resources Research*, *24*(5), 713–722. doi: 10.1029/WR024i005p00713

Kauzmann, W. (2012). Molecular collisions and the transport properties of gasses. In *Kinetic theory of gasses* (chap. 5). Mineola, New York: Dover Publications, Inc.

Lacey, G. (1930). Stable channels in alluvium. *Minutes of the Proceedings of the Institution of Civil Engineers, Thomas Telford-ICE Virtual Library*, *229*, 259–292.

Lajeunesse, E., Malverti, L., & Charru, F. (2010). Bed load transport in turbulent flow at the grain scale: Experiments and modeling. *Journal of Geophysical Research: Earth Surface*, *115*(4). doi: 10.1029/2009JF001628

Langbein, W. B., & Leopold, L. B. (1968). River channel bars and dunes - Theory of kinematic waves. *U.S. Geological Survey Professional Paper 422-L.*

Leary, K. C. P., & Ganti, V. (2020). Preserved fluvial cross strata record bedform disequilibrium dynamics. *Geophysical Research Letters*, *47*(2). doi: 10.1029/2019GL085910

Leclair, S. F., & Bridge, J. S. (2001). Quantitative interpretation of sedimentary structures formed by river dunes. *SEPM Journal of Sedimentary Research*, *71*(2), 713–716. doi: 10.1306/D4268D79-2B26-11D7-8648000102C1865D

Leeder, M. R. (1980). Discussion of the stability of lower stage plane beds and the absence of current ripples in coarse sands. *Journal of the Geological Society*, *138*(6), 753–754. doi: 10.1144/gsjgs.138.6.0753

Liu, M. X., Pelosi, A., & Guala, M. (2019). A statistical description of particle motion and rest regimes in open-channel flows under low bedload transport. *Journal of Geophysical Research: Earth Surface*, *124*(11), 2666–2688. doi: 10.1029/2019JF005140

Mahon, R. C., & McElroy, B. (2018). Indirect estimation of bedload flux from modern sand-bed rivers and ancient fluvial strata. *Geology*, *46*(7), 579–582. doi: 10.1130/G40161.1

Marshall, J. S. (2011). Viscous damping force during head-on collision of two spherical particles. *Physics of Fluids*, *23*(1), 013305. doi: 10.1063/1.3546094

McLean, S. R. (1990). The stability of ripples and dunes. *Earth-Science Reviews*, *29*(1-4), 131–144. doi: 10.1016/0012-8252(0)90032-Q

Métivier, F., Lajeunesse, E., & Devauchelle, O. (2017). Laboratory rivers: Lacey's law, threshold theory, and channel stability. *Earth Surface Dynamics*, *5*, 187–198. doi: 10.5194/esurf-5-187-2017

Oesterle, B., & Petitjean, A. (1993). Simulation of particle-to-particle interactions in gas solid flows. *International Journal of Multiphase Flow*, *19*(1), 199–211. doi: 10.1016/0301-9322(93)90033-Q

Paola, C., & Borgman, L. (1991). Reconstructing random topography from preserved stratification. *Sedimentology*, *38*(4), 553–565. doi: 10.1111/j.1365-3091.1991.tb01008.x

Parker, G., Wilcock, P. R., Paola, C., Dietrich, W. E., & Pitlick, J. (2007). Physical basis for quasi-universal relations describing bankfull hydraulic geometry of single-thread gravel bed rivers. *Journal of Geophysical Research*, *112*(F4), F04005. doi: 10.1029/2006JF000549

Rapp, B. E. (2017). Fluids. In *Microfluidics: Modelling, mechanics and mathematics* (pp. 243–263). Oxford, UK: Elsevier. doi: 10.1016/B978-1-4557-3141-1.50009-5

Raudkivi, A. J. (1963). Study of sediment ripple formation. *Journal of the Hydraulic Divivision of the American Society of Civil Engineers*, *89*(6), 15–34.

Raudkivi, A. J. (1966). Bed forms in alluvial channels. *Journal of Fluid Mechanics*, *26*(3), 507–514. doi: 10.1017/S0022112066001356

Schindelin, J., Arganda-Carreras, I., Frise, E., Kaynig, V., Longair, M., Pietzsch, T., ... Cardona, A. (2012). Fiji: an open-source platform for biological-image analysis. *Nature Methods*, *9*(7), 676–682. doi: 10.1038/nmeth.2019

Schmeeckle, M. W., Nelson, J. M., Pitlick, J., & Bennett, J. P. (2001). Interparticle collision of natural sediment grains in water. *Water Resources Research*, *37*(9), 2377–2391. doi: 10.1029/2001WR000531

Schumm, S. (1960). The shape of alluvial channels in relation to sediment type. *U.S. Geological Survey Professional Paper 352-B*.

Seminara, G., Colombini, M., & Parker, G. (1996). Nearly pure sorting waves and formation of bedload sheets. *Journal of Fluid Mechanics*, *312*, 253–278. doi: 10.1017/S0022112096001991

Shinbrot, T. (1997). Competition between randomizing impacts and inelastic collisions in granular pattern formation. *Nature*, *389*(6651), 574–576. doi: 10.1038/39264

Smith, J. D., & Mclean, S. R. (1977). Spatially averaged flow over a wavy surface. *Journal of Geophysical Research*, *82*(20). doi: 10.1029/JC082i012p01735

Sommerfeld, M. (2001). Validation of a stochastic Lagrangian modelling approach for inter-particle collisions in homogeneous isotropic turbulence. *International Journal of Multiphase Flow*, *27*(10), 1829–1858. doi: 10.1016/S0301-9322(01)00035-0

Southard, J. B., & Boguchwal, L. A. (1990). Bed configurations in steady unidirectional water flows. Part 2. Synthesis of flume data. *Journal of Sedimentary Petrology*, *60*(5), 658–679. doi: 10.1306/212f9241-2b24-11d7-8648000102c1865d

Southard, J. B., & Dingler, J. R. (1971). Flume study of ripple propagation behind mounds on flat sand beds. *Sedimentology*, *16*, 251–263. doi: 10.1111/j.1365-3091.1971.tb00230.x

Strom, K., Papanicolaou, A. N., Evangelopoulos, N., & Odeh, M. (2004). Microforms in gravel bed rivers: Formation, disintegration, and effects on bedload transport. *Journal of Hydraulic Engineering*, *130*(6), 554–567. doi: 10.1061/(ASCE)0733-9429(2004)130:6(554)

Tinevez, J., Perry, N., Schindelin, J., Hoopes, G. M., Reynolds, G. D., Laplantine, E., ... Eliceiri, K. W. (2017). TrackMate: An open and extensible platform for single-particle tracking. *Methods*, *115*, 80–90. doi: 10.1016/j.ymeth.2016.09.016

Van den Berg, J. H., & Van Gelder, A. (1993). A new bedform stability diagram, with emphasis on the transition of ripples to plane bed in flows over fine sand and silt. In *Alluvial sedimentation* (pp. 11–21). Oxford, UK: Blackwell Publishing Ltd. doi: 10.1002/9781444303995.ch2

van Rijn, L. (1984). Sediment transport, part III: Bed forms and alluvial roughness. *Journal of Hydraulic Engineering*, *110*(12), 1733–1755.

Venditti, J. G., Church, M., & Bennett, S. J. (2005b). On the transition between 2D and 3D dunes. *Sedimentology*, *52*(6), 1343–1359. doi: 10.1111/j.1365-3091.2005.00748.x

Venditti, J. G., Church, M., & Bennett, S. J. (2006). On interfacial instability as a cause of transverse subcritical bed forms. *Water Resources Research*, *42*(7), 1–10. doi: 10.1029/2005WR004346

Venditti, J. G., Church, M. A., & Bennett, S. J. (2005a). Bed form initiation from a flat sand bed. *Journal of Geophysical Research: Earth Surface*, *110*(1), 1–19. doi: 10.1029/2004JF000149

Venditti, J. G., Nelson, P. A., & Dietrich, W. E. (2008). The domain of bedload sheets. *Marine and River Dune Dynamics*, 175–183.

Whiting, P. J., & Dietrich, W. E. (1990). Boundary shear stress and roughness over mobile alluvial beds. *Journal of Hydraulic Engineering*, *116*(12), 1495–1511. doi: 10.1061/(ASCE)0733-9429(1990)116:12(1495)

Whiting, P. J., Dietrich, W. E., Leopold, L. B., Drake, T. G., & Shreve, R. L. (1988). Bedload sheets in heterogeneous sediment. *Geology*, *16*(2), 105–108. doi: 10.1130/0091-7613(1988)016⟨0105:BSIHS⟩2.3.CO;2

Wiberg, P. L. (1987). *Mechanics of bedload sediment transport* (Ph.D. Dissertation). University of Washington.

Wiberg, P. L., & Smith, J. D. (1985). A theoretical model for saltating grains in water. *Journal of Geophysical Research*, *90*(C4), 7341. doi: 10.1029/JC090iC04p07341

Wiberg, P. L., & Smith, J. D. (1989). Model for calculating bed load transport of sediment. *Journal of Hydraulic Engineering*, *115*(1), 101–123. doi: 10.1061/(ASCE)0733-9429(1989)115:1(101)

Wilkerson, G. V., & Parker, G. (2010). Physical basis for quasi-universal relationships describing bankfull hydraulic geometry of sand-bed rivers. *Journal of Hydraulic Engineering*, *137*(7), 739–753. doi: 10.1061/(ASCE)HY.1943-7900.0000352

Williams, P. B., & Kemp, P. H. (1971). Initiation of ripples on flat sediment beds. *Journal of the Hydraulic Divivision of the American Society of Civil Engineers*, *97*(4), 502–522.

Wong, M., & Parker, G. (2006). Reanalysis and correction of bed-load relation of Meyer-Peter and Müller using their own database. *Journal of Hydraulic Engineering*, *132*(11), 1159–1168. doi: 10.1061/(ASCE)0733-9429(2006)132:11(1159)

Wright, S. A., & Parker, G. (2004). Flow resistance and suspended load in sand-bed rivers: Simplified stratification model. *Journal of Hydraulic Engineering*, *130*(8), 796–805. doi: 10.1061/(ASCE)0733-9429(2004)130:8(796)